JGR Oceans

RESEARCH ARTICLE
10.1029/2019JC015650

Key Points:
- Interactions between phytoplankton and bottom oxygen are identified with high-quality satellite chlorophyll data and field observations
- Particle dislocation effect is significant throughout the year and agrees with seasonal circulation patterns
- Satellite chlorophyll data derived with the absorption-based approach can be used as an indicator for changes in bottom oxygen demand

Supporting Information:
- Supporting Information S1
- Figure S1
- Figure S2
- Figure S3
- Figure S4
- Figure S5

Correspondence to:
G. Zheng,
guangming.zheng@noaa.gov

Citation:
Zheng, G., & DiGiacomo, P. M. (2020). Linkages between phytoplankton and bottom oxygen in the Chesapeake Bay. *Journal of Geophysical Research: Oceans*, *125*, e2019JC015650. https://doi.org/10.1029/2019JC015650

Received 13 SEP 2019
Accepted 9 JAN 2020
Accepted article online 16 JAN 2020

Linkages Between Phytoplankton and Bottom Oxygen in the Chesapeake Bay

Guangming Zheng[1,2] **and Paul M. DiGiacomo**[1]

[1]NOAA/NESDIS Center for Satellite Applications and Research, College Park, MD, USA, [2]Cooperative Institute for Satellite Earth System Studies, Earth System Science Interdisciplinary Center, University of Maryland, College Park, MD, USA

Abstract The primary cause of coastal hypoxia is generally attributed to phytoplankton blooms and their subsequent benthic decay. However, direct linkages between phytoplankton and hypoxia have been rarely reported. Here using satellite and field data, we show that such linkages exist in the Chesapeake Bay. For deeper (>10 m) but nonhypoxic stations, bottom dissolved oxygen is significantly correlated with surface algal biomass during the preceding weeks. Optimal correlation exhibits a bimodal seasonal variation with two peaks in April and August, respectively. Significant particulate dislocation effect is also observed: In April, May, August, and September when water column is stratified, the most significant influencer of bottom oxygen is attributable to phytoplankton blooms located down-estuary; during destratified months of October and November, however, the dislocation effect switches to the opposite direction, that is, phytoplankton from up-estuary have the biggest impact. We also notice enhanced phytoplankton growth posterior to lower bottom oxygen, and the strongest correlation is during summer when release of recycled ammonium and hypoxia-induced phosphate is the most intense. These results demonstrate that the decay of phytoplankton exerts a significant impact on bottom oxygen and releases ammonium which sustains further bloom, whereas hypoxia promotes phytoplankton growth by enhancing the efficiency of phosphate recycling. Importantly, the capability of using satellite data to capture these linkages has significant ramifications for improving hypoxia forecasts in coastal systems. It essentially provides a way to characterize and constrain changes in bottom oxygen demand.

1. Introduction

Hypoxia in aquatic ecosystems refers to the depletion of dissolved oxygen (DO) to levels that are detrimental to organisms living in the systems, which occurs when oxygen consumption exceeds its resupply for a prolonged period of time. It has been an increasing global concern in the past several decades, constantly expanding to new areas that had never experienced hypoxia before (Breitburg et al., 2018; Diaz & Rosenberg, 1995, 2008; Diaz, 2001). This expansion has been largely driven by climate change (Deutsch et al., 2011; Hoegh-Guldberg & Bruno, 2010) and is expected to continue to worsen in the future. For example, changes in wind and currents driven by anthropogenic climate change can lead to intensified upwelling and thereby increase primary production, the sinking flux of organic matter, and the incidence of hypoxic events in the ocean (Hoegh-Guldberg & Bruno, 2010). In coastal waters, anticipated increases in both total and extreme precipitation (Sinha et al., 2017) are likely to exacerbate hypoxia through intensified stratification and nutrient loading. Expanding hypoxia, along with ocean warming and ocean acidification, is considered to be one of the three primary ocean consequences of rising atmospheric CO_2 (Levin & Breitburg, 2015). Therefore, there is a pressing need to further understand the mechanisms that lead to hypoxia and, ultimately, to accurately forecast hypoxic events.

Hypoxia is associated with the sinking flux of organic matter sustained by surface particulate organic matter (POM). The primary POM source that fuels coastal hypoxia has been widely associated with algal growth driven by nutrient loadings. Although terrestrial POM sources including riverine discharge and lateral transport from coastal wetlands (Bauer et al., 2013) can also be important, the generally accepted hypothesis is that nutrient loadings trigger the production of planktonic organic matter which eventually sinks to the bottom, decomposes, and depletes DO (e.g., Bauer et al., 2013; Cai et al., 2011). Indeed, a number of studies have shown the correlation between total area or volume of hypoxia and river streamflow or nutrient loadings (e.g., Bianchi et al., 2010; Hagy et al., 2004). Therefore, in principle, there should also be an appreciable linkage between phytoplankton and hypoxia, and since chlorophyll-*a* concentration (Chl-*a*) can be

quantified from space, the monitoring and forecast of coastal hypoxia might be improved with satellite Chl-*a* data. However, the linkage between phytoplankton and coastal hypoxia has been incompletely addressed.

Multiple reasons may explain the limited evidence showing the relationship between phytoplankton and hypoxia. Since hypoxia represents a cumulative effect of organic deposition and decomposition over a period of weeks or even months, in situ sampling methods are subject to both spatial and temporal undersampling issues. Satellite remote sensing does provide extensive coverage, however, standard ocean color Chl-*a* products are likely inadequate to study this linkage for coastal waters (e.g., Walker & Rabalais, 2006) owing to their optical complexities. Water-leaving light detectable from satellite is contributed not only by phytoplankton but also from nonalgal pigmented agents that have originated from terrestrial sources such as humic particles, mineral particles, and dissolved humic matter (Zheng & DiGiacomo, 2017b). As a result, standard Chl-*a* products are subject to accuracy issues associated with the misattribution of nonalgal optical signals to phytoplankton.

The Chesapeake Bay is a prominent example of such complexities with the largest watershed-to-water ratio by area (14:1) among major coastal water bodies in the world. Seasonal hypoxia has been worsening in the bay since the 1930s (Hagy et al., 2004), and its main cause was believed to be eutrophication-induced algal proliferation (Kemp et al., 2005; Officer et al., 1984). In this study, we revisit the linkage between surface phytoplankton and bottom oxygen in the Chesapeake Bay using satellite data processed with algorithms tailored for this region (Zheng & DiGiacomo, 2017a; Zheng et al., 2015), notably an algorithm capable of separating the light absorption signals of phytoplankton, nonalgal particulate, and dissolved organic matter (Zheng et al., 2015). This feature alleviates the interference from nonalgal materials and enables a more accurate Chl-*a* product. Can this algorithm help capture the linkage between phytoplankton and hypoxia in this region? Answering this question is important not only to advance our understanding of the interaction between phytoplankton and hypoxia but also to test whether satellite Chl-*a* data can be useful to constraining the sinking flux of oxygen-consuming organic matter. This is the focus of this study.

2. Data and Methods

Three data sets were assembled in this study using both field-measured and satellite-derived data. The first data set comprises 632 pairs of coincident matchups of field-measured biogeochemical variables and satellite-derived inherent optical properties (IOPs). A valid matchup was defined by both time and location as when field and satellite observations were made within 3 hr and 1 km. The purpose of this data set is to evaluate which optical variable is best suited for characterizing POM in the study area. This evaluation is necessary because nonalgal POM sources such as river discharge and coastal wetlands (covering ~10% of the bay area) can be important in the Chesapeake Bay. Field-measured biogeochemical variables include concentrations of surface particulate organic carbon (POC) and suspended particulate matter (SPM). Satellite-derived IOPs include the absorption coefficients of phytoplankton, $a_{\mathrm{ph}}(\lambda)$, nonalgal particles, $a_d(\lambda)$, and colored dissolved organic matter, $a_g(\lambda)$, as well as the total particulate backscattering coefficient, $b_{\mathrm{bp}}(\lambda)$ at 445 nm, where λ denotes light wavelength in vacuum. The 445-nm band is chosen because both algal and nonalgal particles exhibit significant absorption at this wavelength.

The second data set comprises 2,352 pairs of colocated field and satellite observations and allows us to study the interplay between phytoplankton and DO in the Chesapeake Bay. Specifically, the data include field-measured bottom DO concentration and daily time series of satellite-derived surface Chl-*a* at 38 field stations (Figure 1). Each Chl-*a* time series spans from 30 weeks before to 30 weeks after the corresponding DO observation to cover sufficiently long time window for observing potential effects and feedback. To reduce noise, we binned the daily Chl-*a* observations into weekly averages and obtained weekly time series. The daily data set comprises 23% valid Chl-*a* retrievals with the rest of data missing due to various issues such as fog, cloud coverage, high turbidity, and proximity to land. So on average, each weekly binned data point contains 1.6 valid daily values.

The third data set is used to study potential effects of particle dislocation on bottom oxygen. This data set is similar to the second one with two exceptions. First, it is only sampled along the main stem stations that are deeper than 10 m and only the middle 14 stations (see black solid line in Figure 1) in order to leave enough distance to sample Chl-*a* data in both up-estuary and down-estuary directions along the main stem. Second, the Chl-*a* is not necessarily collocated with DO sampling which is fixed at the field stations but instead sampled from 70 km up-estuary of the DO to 50 km down-estuary by at 2-km incremental interval, that is,

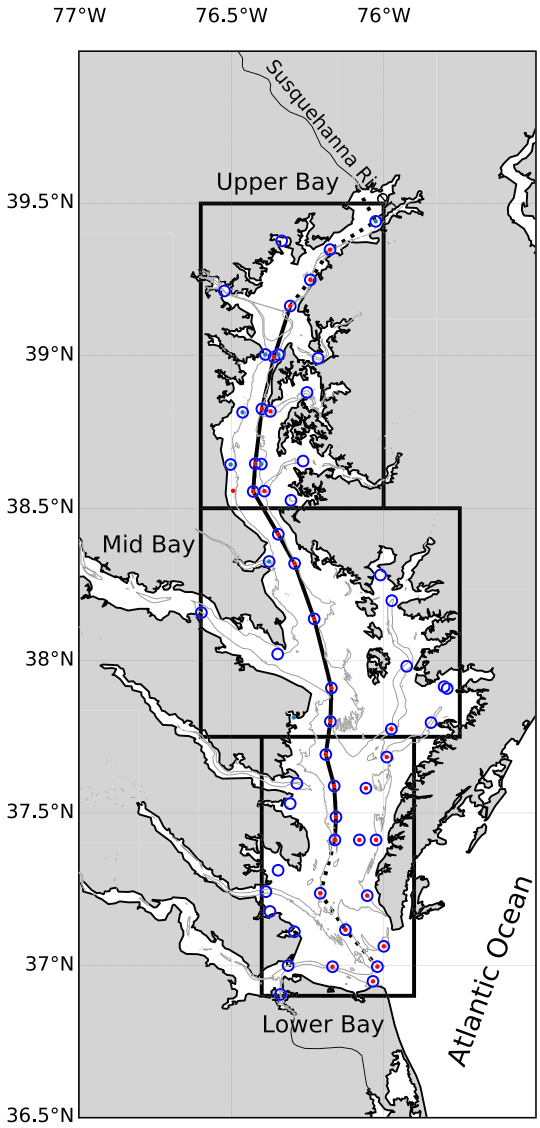

Figure 1. Locations of Chesapeake Bay Program field sampling stations. Open circles represent sampling stations of particulate organic carbon and suspended particulate matter; dots for bottom DO and nutrients, with blue dots denoting stations shallower than 10 m and red dots deeper than 10 m. Thin light gray curves denote the 10 m bathymetry. The axial solid and dotted lines represent the main stem transect. Only field data from stations on the solid line are used for constructing the third data set (section 2) used for particle dislocation analysis (section 3.3). Boxes mark the upper, middle, and lower Chesapeake Bay. Land is masked as light gray.

at 61 different locations for each DO station. We found 1,633 entries of field-measured DO data; so in total $1{,}633 \times 61$ pairs of DO and Chl-*a* time series were analyzed. Data density for this data set varies with spatial shifts. For example, the percentage of valid daily Chl-*a* retrievals at 70 km up-estuary, 0 km (no spatial shift), and 50 km down-estuary are 24%, 31%, and 27%, respectively. So on average, each weekly binned data point contains 1.7–2.2 valid daily values. Below we describe the field and satellite data in details.

2.1. Field Data

All field data were obtained from the Chesapeake Bay Program (CBP), a long-term field sampling network covering the entire Chesapeake Bay. Sampling stations where data used in this study were collected are shown in Figure 1. For this study we used data collected between November 2011 and December 2017, consistent with the temporal span of our satellite data. The POC was determined by combusting particulates retained on filter pad at 975–1050 °C using an elemental analyzer, assuming that all of the particulate carbon is in organic form. The resultant POC values may thus include some contribution from inorganic

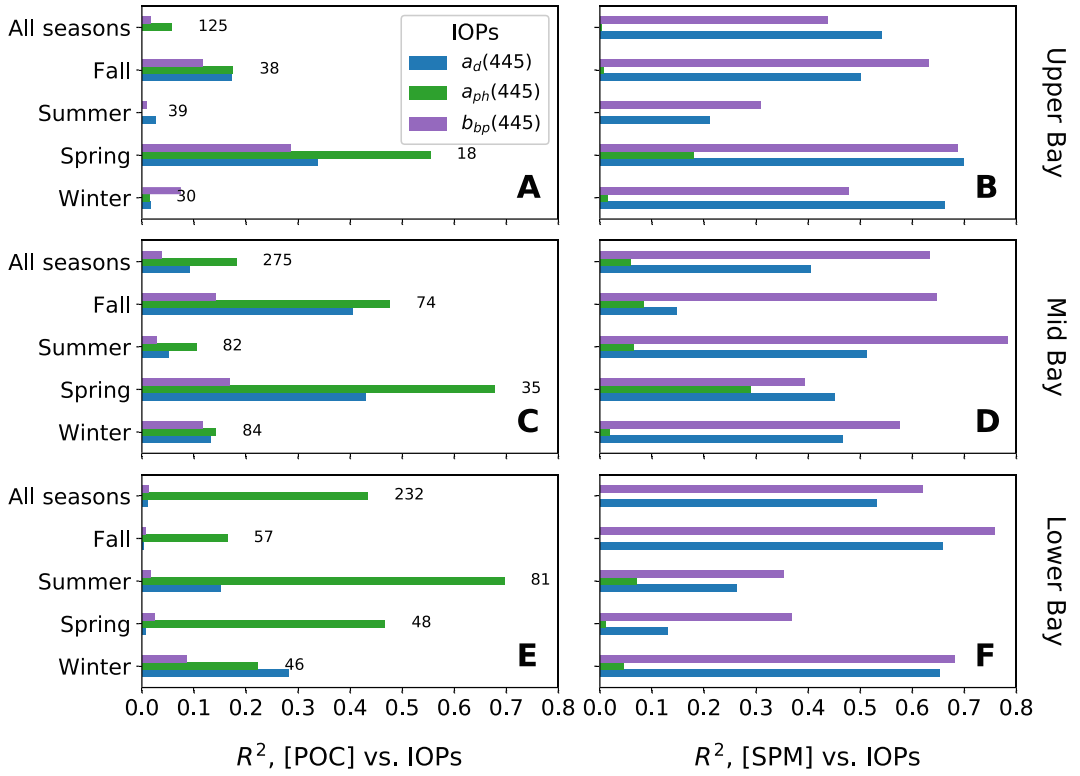

Figure 2. (a–f) Correlation coefficients between POC, SPM, and IOPs of surface water samples in Chesapeake Bay. Numbers to the right of bars indicate the number of matchups for each season and bay section, which is the same for all variables shown here.

carbon. The SPM was determined gravimetrically by filtering water samples through preweighed filters and reweighing them after being dried at 103–105 °C. The DO was measured in situ at each station using either a Clark cell (polarographic) or luminescent optical sensor. Sensors were calibrated at the beginning and end of each sampling cruise according to manufacturers specifications. Other ancillary field data used here include concentrations of ammonium [NH_4^+] and dissolved orthophosphate [PO_4^-] at the bottom of water column. Ammonium was determined directly with an autoanalyzer using the automated alkaline phenol hypochlorite method (EPA 350.1 or equivalent, ODell, 1993a). Dissolved orthophosphate was measured with an ascorbic acid reduction method with an autoanalyzer, following EPA method 365 (ODell, 1993b).

2.2. Satellite Data

The satellite data were collected with the Visible Infrared Imaging Radiometer Suite (VIIRS) onboard Suomi National Polar-orbiting Partnership from 2011 to 2017. The processing of VIIRS $R_{rs}(\lambda)$ data followed the same procedure as detailed in a previous work (Zheng & DiGiacomo, 2017a), and here we provide only a brief description from a dataflow standpoint. First, raw data from VIIRS were processed into the spectral remote sensing reflectance, $R_{rs}(\lambda)$, data following a processing version of "SCI_OC04.0_V1.20." We used data obtained with the "BMW" atmospheric correction algorithm (Jiang & Wang, 2014) which is similar to using the near-infrared bands as a basis for making the "black-pixel" assumption. Second, the $R_{rs}(\lambda)$ data were screened using a scoring system (Wei et al., 2016) and only the most highly scored data were accepted. Next, the quality-controlled reflectance data were inverted with the quasi-analytical algorithm, version 6 (Lee, 2014), to obtain the total nonwater absorption, $a_{nw}(\lambda)$, and particulate $b_{bp}(\lambda)$ coefficients. The Generalized Stacked Constraints Model (Zheng et al., 2015) was subsequently used to partition the $a_{nw}(\lambda)$ into algal $a_{ph}(\lambda)$, nonalgal particulate $a_d(\lambda)$, and dissolved organic $a_g(\lambda)$ components. Finally, the Chl-*a* was calculated simply by multiplying $a_{ph}(\lambda)$ at 672 nm, which is near the red peak of algal absorption, with a multiplication factor of 100 mg/m^2 based on a recently developed Chl-*a* algorithm tailored for the Chesapeake Bay (Zheng & DiGiacomo, 2017a).

3. Results and Discussion

3.1. Selection of Optical Indicator of POM

The first problem that needs to be addressed is which satellite-derived IOP is best suited as indicator of surface POM in the Chesapeake Bay. Since total particulate backscattering coefficient, $b_{bp}(445)$, tends to be dominated by minerals (Zheng & DiGiacomo, 2017b) particularly in mineral-laden estuarine waters, this problem effectively distills down to the selection among two particulate absorption coefficients, namely, $a_{ph}(\lambda)$ and $a_d(\lambda)$. Figure 2 shows the degree of correlation between field-measured POC and and satellite-derived $a_{ph}(\lambda)$ and $a_d(\lambda)$ at the 445-nm band across different sections of the bay and different seasons of the year. For comparison, satellite-derived $b_{bp}(445)$ and field-measured SPM were also included, whose strong correlation also confirms the domination of minerals in $b_{bp}(445)$. The results for dissolved organic absorption $a_g(445)$ suggest very low correlations with POC, which are expected and not shown.

We found that total POC correlates significantly better with $a_{ph}(445)$ than with $a_d(445)$, and the degree of correlation increases from upper to lower bay as terrestrial influence decreases (Figures 2a, 2c, and 2e). Although we cannot rule out the significance of terrestrial allochthonous POM, the better $a_{ph}(445)$-POC correlation is most likely owing to the dominant role played by phytoplankton-derived autochthonous POM in the total POM pool in most of the Chesapeake Bay. Previous in situ work conducted in this area demonstrates that suspended organic particles in the Chesapeake Bay, particularly the lower bay, are derived mainly from autochthonous sources, primarily phytoplankton and bacteria (Canuel & Zimmerman, 1999; Zimmerman & Canuel, 2001), whereas terrestrial organic particles from the Susquehanna River are likely trapped and buried within the upper reach of the bay, a small area up-estuary of the turbidity maximum zone (Zimmerman & Canuel, 2001).

The $a_d(445)$, contributed by both humic and mineral particles, can occasionally correlate well with POC for certain seasons and sections (e.g., spring and fall in middle bay) presumably when organic detritus is abundant in water. Overall, however, the correlation between $a_d(445)$ and POC appears to be subject to significant interference from absorbing minerals. As shown in Figures 2b, 2d, and 2f, $a_d(445)$ exhibits a comparable degree of correlation with SPM compared with the mineral-dominated $b_{bp}(445)$.

These results suggest that in the Chesapeake Bay POM is likely dominated by autochthonous matter associated with phytoplankton despite the potentially significant influence from river discharge and coastal wetlands. The degree of correlation between POC and $a_{ph}(\lambda)$ derived with our approach is reasonable considering the uncertainties involved in the collection and processing of both field and satellite data, and the $a_{ph}(\lambda)$ can be used as an indicator of surface POM in the Chesapeake Bay. For simplicity, below we use Chl-*a* converted from $a_{ph}(\lambda)$ at the 672-nm band using a local algorithm (Zheng & DiGiacomo, 2017a) to characterize the dynamics of POM and phytoplankton biomass.

3.2. Influence of Surface Phytoplankton on Bottom Oxygen

We established 38 virtual stations collocated with CBP field stations (Figure 1) in the Chesapeake Bay proper and analyzed the relationship between bottom DO concentration and multiweekly mean surface Chl-*a* before and after the DO observations. In this section we focus on the cumulative effect of surface Chl-*a* before DO sampling, hereafter referred to as pre-DO Chl-*a*. The pre-DO Chl-*a* discussed in this section is sampled at the same location of DO. Potential particle dislocation effect will be addressed in the next section. In general, the relationship between DO and pre-DO Chl-*a* exhibits great seasonal variability. During warmer months, there are patterns of covariation which are exemplified by Figure 3 using the pre-DO Chl-*a* averaged for the immediate 4 weeks preceding DO sampling. During cooler months, the correlation between the two is weaker (results not shown). This is because DO is controlled by both oxygen supply and consumption. Whereas oxygen consumption is associated with phytoplankton-derived organic matter, oxygen supply is determined mainly by advection and vertical mixing related to currents, water column stability, and physical forcings (Li et al., 2015; Scully, 2013). In cooler months when water column is unstable, vertical mixing overwhelms oxygen consumption and appears to be the dominant factor affecting DO. Therefore, for the purpose of this study, we focus on warmer months when the water column is generally stratified, so that the effect of vertical mixing is relatively limited and the effect of phytoplankton-derived organic matter is more appreciable.

To highlight major patterns of data distribution, a kernel density estimation tool provided by Python "Seaborn" library was applied to the original data. The kernel density estimation is achieved by first splitting the *x* and *y* axes into multiple bins, counting the number of data points in each bin and then fitting the

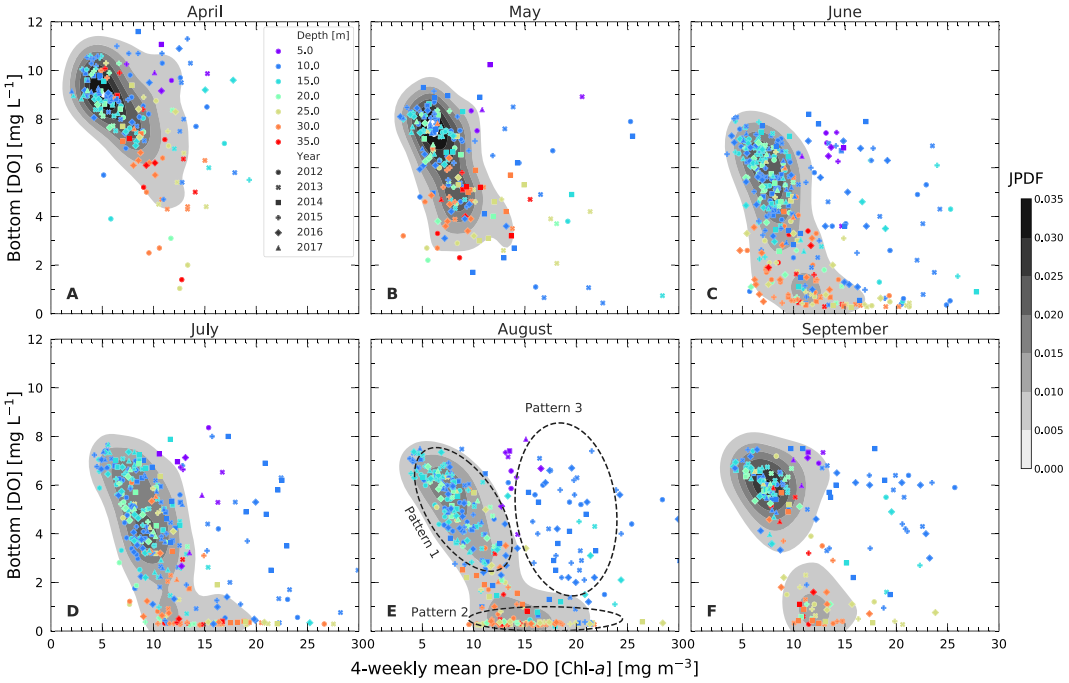

Figure 3. (a–f) Relationship between DO at the bottom and 4-weekly mean pre-DO Chl-*a* at the surface in the Chesapeake Bay during main hypoxia season. Data are categorized by year and bottom depth of each station. JPDF, joint probability density function generated from the kernel density estimation; the unit is probability per unit area in the plane defined by the *x* and *y* dimensions.

counts per bin with multiple bivariate Gaussian functions (kernels). The resultant joint probability density function (gray shades in Figure 3) essentially maps out the 2-D probability distribution of data points.

Figure 3 demonstrates three main patterns with respect to the relationship between DO and pre-DO Chl-*a*. Pattern 1 is the trend of decreasing DO with increasing pre-DO Chl-*a* as indicated by the upper parts of the gray areas with higher joint probability density function (see example in Figure 3e). When anoxic condition (zero DO) is reached or approached, the pre-DO Chl-*a* no longer matters as oxygen is unavailable for further consumption (Pattern 2, Figure 3e). This usually happens to deeper stations where replenishment of oxygen from surface oxygenated water is more difficult. Conversely, bottom waters at shallower stations are prone to vertical ventilation and can often defy Patterns 1 and 2 by exhibiting high DO even when pre-DO Chl-*a* is high (Pattern 3, Figure 3e). This usually happens for stations shallower than 10 m, but occasionally deeper stations also fall within this pattern.

In the case of both Patterns 2 and 3, sinking POC flux associated with surface algae becomes irrelevant with respect to short-term changes in bottom DO because there is either too little (Pattern 2) or too much (Pattern 3) oxygen supply to bottom water relative to the magnitude of POC flux. Only cases with balanced oxygen supply and consumption as those found in Pattern 1 make it possible for bottom DO to respond noticeably to variation of POC flux, thus are suitable for quantifying the influence of surface algae on bottom oxygen.

So next we limit our analyses only to data that fall within Pattern 1. This was done by excluding data with near-anoxic conditions (DO≤1 mg/L) or too high pre-DO Chl-*a* (>15 mg/m^3) to avoid Pattern 2 and data from nine shallow stations with bottom depth ≤10 m to avoid Pattern 3, although the latter would cause some loss of data that fall in Pattern 1. A closer look at these data suggests that the correlation between Chl-*a* and DO exists primarily spatially across different stations for a given year and, to a lesser extent, temporally across different years for a given station, with monthly variation in the relative degree of spatial and temporal correlations (Figures S1–S4 in the supporting information). For example, in April both spatial and temporal correlations are significant, but in August the spatial correlation dominates the overall correlation owing to the relatively small range of DO variability at each individual station. Regardless of whether spatial or temporal correlation dominates, both types of correlation indicate the influence of phytoplankton-derived organic matter upon bottom oxygen demand and ultimately DO which are driven by the same mechanism.

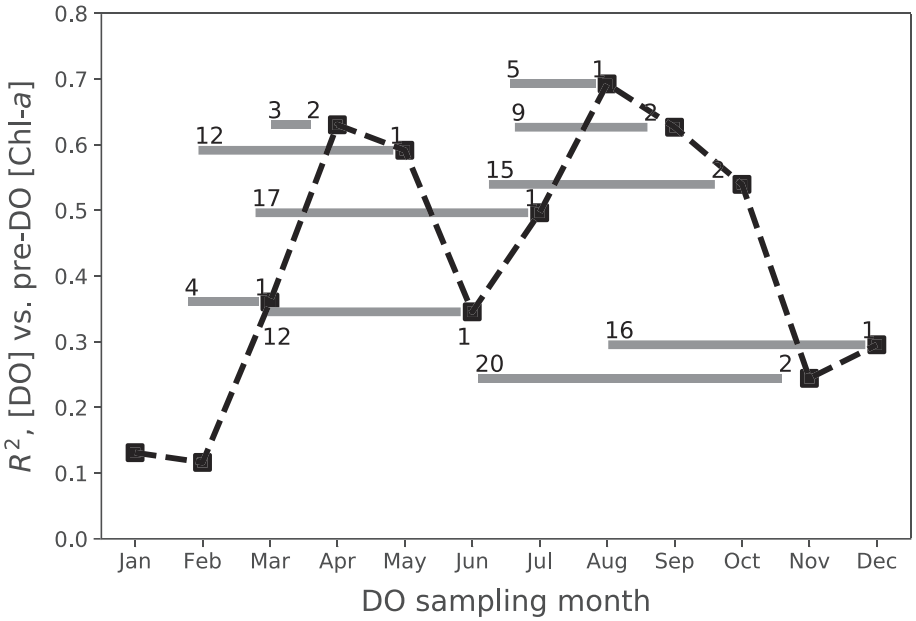

Figure 4. Optimal correlation between DO and mean pre-DO Chl-*a* computed for various duration and time lags at 30 stations deeper than 10 m in the Chesapeake Bay. Gray horizontal bars to the left of R^2 data points denote the duration over which the mean pre-DO Chl-*a* values are calculated; numbers on the bar represent the starting and ending weeks of the duration.

Figure 3 only represents an example of the relationship between DO and pre-DO Chl-*a*. The exact degree of correlation between the two variables for Pattern 1 data is actually time dependent. To identify the optimal degrees of correlation, we analyzed the correlation between DO and pre-DO Chl-*a* calculated with various duration and time lags. We found that the optimal correlation coefficient, R^2, between bottom DO and pre-DO Chl-*a* for data points within Pattern 1 is significant throughout the year except in January and February with two maxima in spring and summer, respectively (Figure 4). The duration and time lag corresponding to the optimal correlation vary from month to month. In early spring (March and April) the duration is short (2–4 weeks), suggesting that bottom DO is most influenced by surface algae during the several weeks preceding it. In May–July, the duration lengthens significantly to 12–17 weeks and always dates back to around March. In other words, bottom DO during this period of time is affected by surface algae across multiple months from March onward. This trend is interrupted in late summer/early fall (August–October) when a pattern similar to that in spring repeats; the duration starts relatively short (5 weeks) in August, increases to 8 weeks in September, and to 14 weeks in October.

Since surface phytoplankton influences bottom oxygen through the provision of sinking POM flux, results shown in Figure 4 imply that the sinking POM flux is seasonally inhomogeneous with some seasonal "hot spots." To pinpoint these hot spots, we examined the relationship between DO and pre-DO Chl-*a* at higher temporal resolution (biweekly). Figure 5 shows that, overall, R^2 between bottom DO and biweekly mean pre-DO Chl-*a* decreases monotonically with time lag for March and April (Figure 5a), and for August and September (Figure 5b), that is, during these months the Chl-*a* immediately preceding the DO sampling generally correlates the best with bottom DO. For other months, the maximum R^2 value exhibits a time lag from DO sampling. Tracing back the timing of maximum R^2 for each month narrows the time windows of the hot spots down to approximately March–April and July–September. This is when phytoplankton-derived POM sinking flux might have been the strongest and nicely matches with local phytoplankton phenology with two major blooms in March and July (Figure S5). The seasonal variability in sinking POM flux should be taken into account in hypoxia forecast models.

Why do seasonal hot spots of sinking POM flux happen in March–April and July–September? The reasons might be associated with well-known ecological processes in this region. In aquatic systems, the sinking POC flux mainly comprises fecal pellets, marine snow, and phytoplankton (Turner, 2002). For the Chesapeake Bay, the spring phytoplankton bloom is typically grazed by a major zooplankton bloom

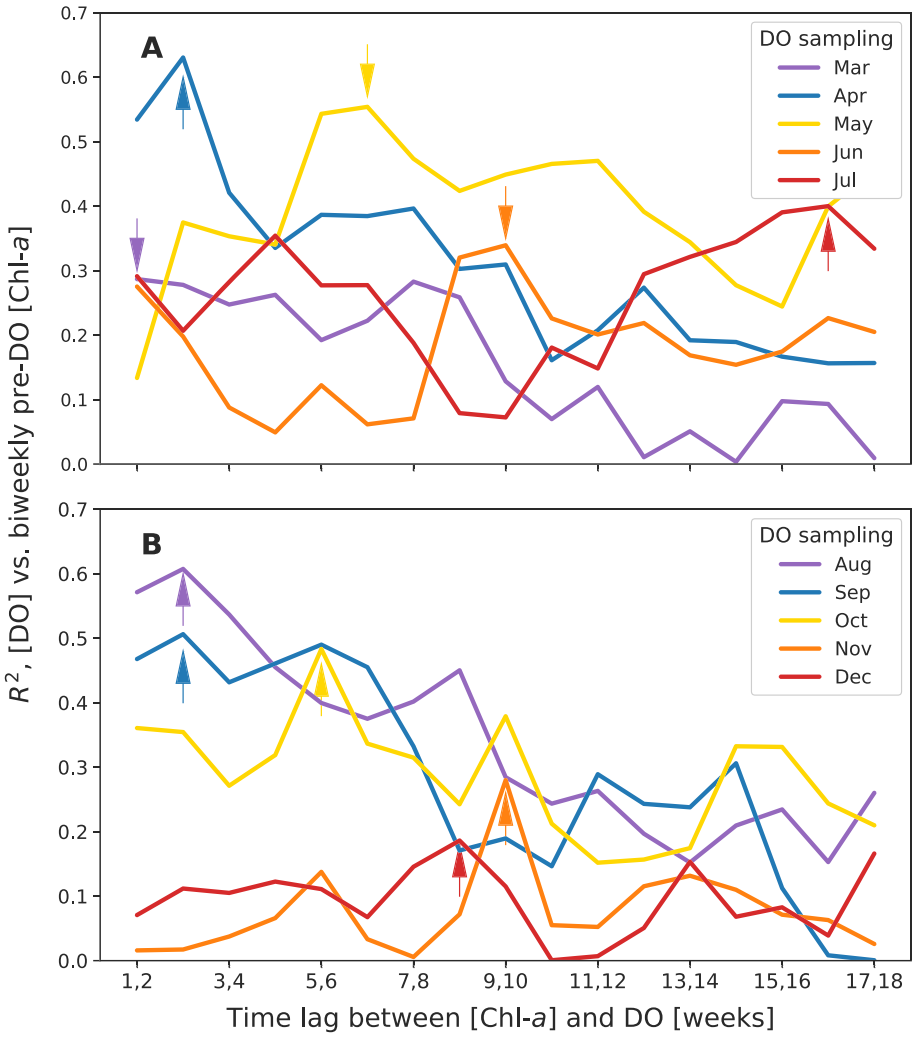

Figure 5. Correlation between DO and biweekly mean pre-DO Chl-*a* as a function of time lag for (a) spring-summer and (b) summer-winter seasons. Arrows mark the maximum R^2 value for each month.

(Baird & Ulanowicz, 1989; Harvey & Johnston, 1995). In addition, grazing by large zooplankton (>200 μm) is significant, sometimes dominant (White & Roman, 1992), which produce larger, faster-sinking fecal pellets capable of reaching the bottom and consuming oxygen there instead of being respired in the upper water column. Even if the grazing of microzooplankton (<200 μm) can also dominate (McManus & Ederington-Cantrell, 1992), their slower-sinking fecal pellets might still manage to sink to the bottom considering the shallowness of the Chesapeake Bay. Therefore, zooplankton fecal pellets might be an important contributor to the March–April hot spot. Another potentially important contributor is the direct sinking of diatoms, which dominate spring bloom in the Chesapeake Bay (Harding Jr et al., 2016; Marshall et al., 2005). Large-scale sedimentation of diatom blooms in spring has been observed in the Chesapeake Bay (Hagy et al., 2005) as well as other coastal waters (Dortch et al., 2013; Turner, 2002), and its contribution to the spring hotspot in the Chesapeake Bay should not be overlooked. With respect to the July–September hot spot, marine snow might have played a major role. Compared with that observed in spring, summer production of zooplankton fecal pellets is greatly reduced owing to top-down control of zooplankton by jellyfish (Baird & Ulanowicz, 1989). Excess primary production which otherwise would have been grazed by zooplankton is partly exuded out as dissolved organic matter, which promotes microbial growth and production of sticky exopolymers, creating favorable conditions for large aggregates to form (Turner, 2002). For example, Harvey and Johnston (Harvey & Johnston, 1995) found that in October large particles in a middle bay bottom water were dominated by aggregates of intact phytoplankton cells and aggregates enriched in polyunsaturated fatty acids.

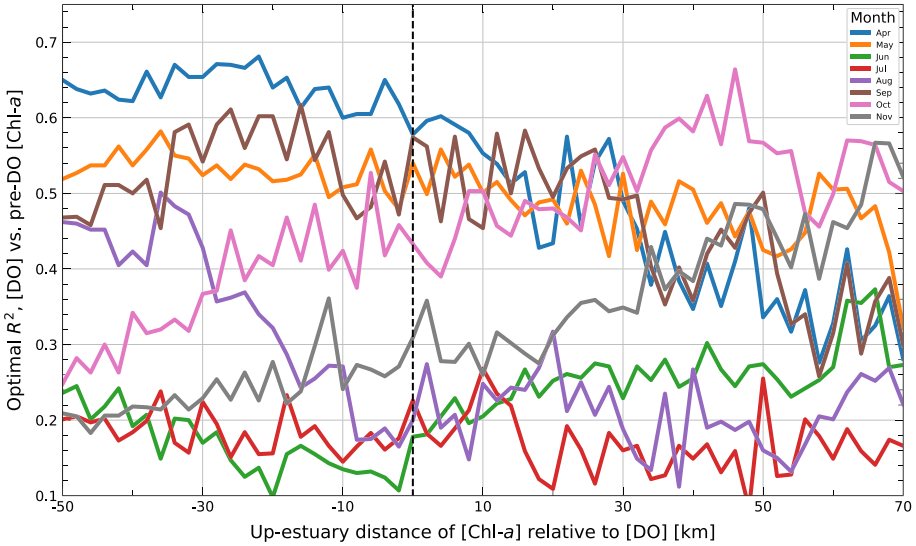

Figure 6. Optimal correlation between DO and pre-DO Chl-*a* as a function of dislocation distance between the two. The distance is calculated as the number of kilometers that the Chl-*a* sampling is up-estuary of the DO sampling. So negative distance corresponds to Chl-*a* sampled down-estuary of DO. Note that the optimal correlations between DO and Chl-*a* are determined independently among different locations and correspond to different time lags (Not shown here. See text for more information.).

3.3. Effect of Particle Dislocation on Bottom Oxygen

The previous section shows the effect of time lag of organic decomposition on bottom oxygen. It is possible that the location where organic particles were generated differs from where they decomposed and consumed oxygen, that is, there might be a dislocation between phytoplankton bloom and hypoxia. In this section, we evaluate this spatial dislocation effect on top of the temporal effect. However, a comprehensive treatment of this problem requires a 3-D hydrodynamic model to track sinking particles and is beyond the scope of this study. Instead, we simplify the problem to 1-D by limiting our analysis to only 14 main stem stations along the central axis of the Chesapeake Bay (Figure 1). For this analysis we sample satellite Chl-*a* data both up-estuary and down-estuary of the in situ DO observations because circulation patterns in the Chesapeake Bay suggest that bottom particles and waters could be transported in either direction. Flow patterns in the Chesapeake Bay averaged over the tidal cycles are mainly affected by stratification, river discharge, and wind. Under stratified conditions, the Chesapeake Bay is a two-layer system; river discharge drives a down-estuary flow at the surface and an up-estuary flow at the bottom in the central channel (Boicourt et al., 2013; Tyler & Seliger, 1978), which can be strengthened by down-estuary wind and weakened or reversed by up-estuary wind, at least in the upper and middle bay (Guo & Valle-Levinson, 2008; Li & Li, 2011; Li et al., 2015). When water column is well mixed, current direction becomes depth independent (Goodrich et al., 1987; Li et al., 2007) and down-estuary transport in the bottom becomes possible. In addition, there is variability in the lateral structure of the circulation field. Lateral transport can be generated by up-estuary winds (Li & Li, 2011; Li et al., 2015), and currents can flow in the opposite directions between the flanks and the central channel under destratified conditions (Guo & Valle-Levinson, 2008). These studies suggest that particles sinking from the surface may undergo complex pathways before they are completely mineralized.

So we calculated the correlation coefficient between DO and pre-DO Chl-*a* with various dislocation distance and time lags for stations along the main stem transect (Figure 1). Note that the three most upper bay stations and three most lower bay stations were excluded from this analysis to obtain the same number of stations for each correlation calculation corresponding to any dislocation distance. Optimal correlation at each dislocation distance is shown in Figure 6.

Figure 6 shows that during April, May, and September, the DO levels along the main stem transect are most correlated with Chl-*a* sampled down-estuary. Higher correlation corresponds to a broad dislocation distance with times lags varying within 1–3, 5–10, and 1–8 weeks, respectively. However, there is a lack of clearly defined peaks (considering random errors). That is, no phytoplankton at a single location exerts a dominant impact on bottom DO at any given location. This is not the case for August, when the dislocation distance of

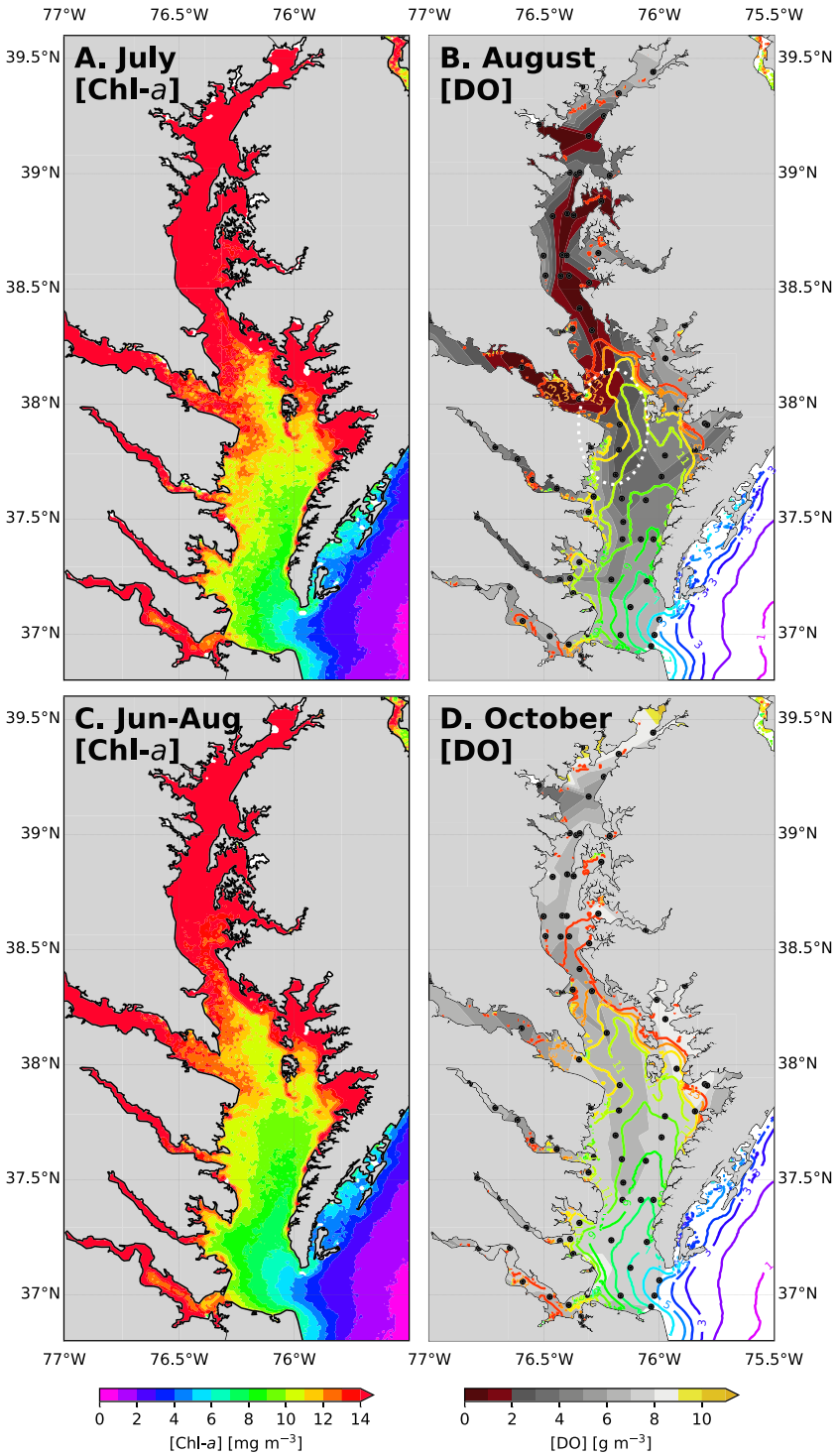

Figure 7. Comparison between VIIRS-derived surface Chl-*a* and field-measured bottom DO for periods when the two variables exhibit optimal correlation along the main stem transect, with the effect of phytoplankton-derived oxygen demand dislocated up-estuary (a and b) or down-estuary (c and d). The DO maps (b and d) are overlaid with contours of the same Chl-*a* used in the panels to the left (a and c) but smoothed with a 5 × 5 median filter to show only the main pattern. The maps show climatologies calculated as their median values during 2011–2017.

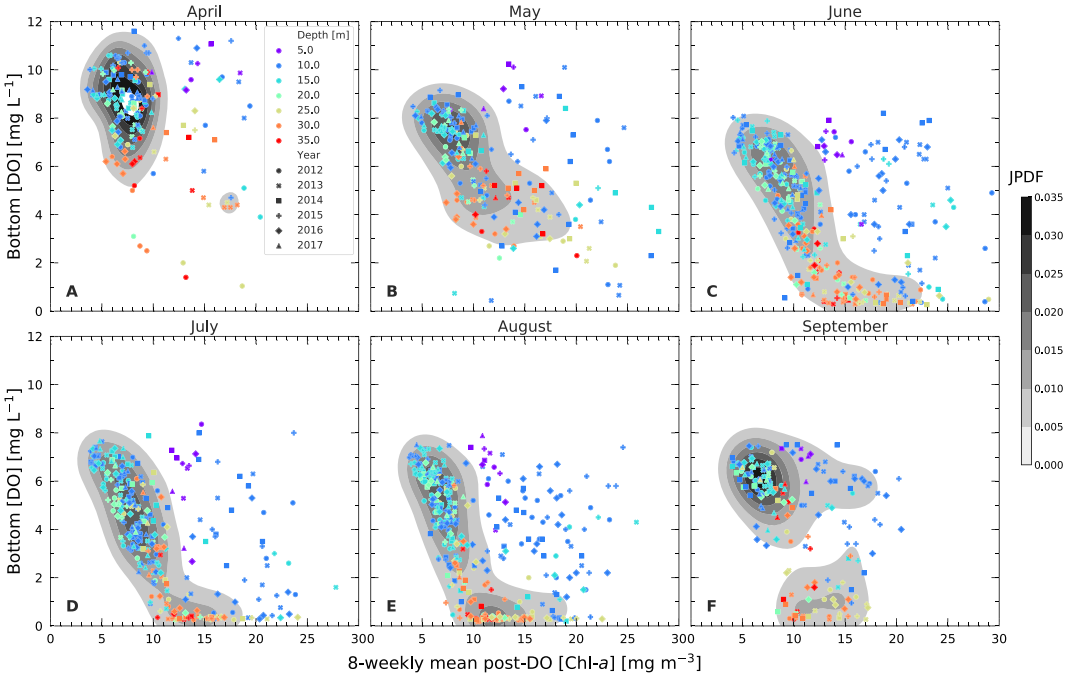

Figure 8. Same as Figure 3 except for 8-weekly mean post-DO Chl-*a*.

optimal correlation is around 36 km down-estuary of DO with a time lag of 1–4 weeks. The ultimate location of optimal correlation may reflect the compounding effects of both particulate and water movements, and it is unclear exactly why a distinct peak of high correlation exists in August but is absent in other months. However, we do note that the direction of dislocation agrees with general circulation pattern during these seasons, which pushes surface Chl-*a* down-estuary and bottom waters up-estuary. The correlation is low in June and July because the dynamic range of DO along the transect during these periods is small.

Opposite dislocation direction is observed after September. In October, bottom DO is most correlated with Chl-*a* sampled 46 km up-estuary, with a significant time lag of 8–15 weeks, that is, around June–August and overlaps with the summer phytoplankton bloom and the second peak of organic sinking flux. In November, the dislocation distance corresponding to optimal correlation is 66–68 km up-estuary with a time lag of 8–10 weeks. The high correlation between DO and up-estuary Chl-*a* can only be explained by a net down-estuary bottom transport in October and November, which is possible because September marks the start of the water column destratification process and the two-layer flow pattern switches to a vertically uniform one (Goodrich et al., 1987). These results also demonstrate that organic matter produced up-estuary during summer controls bottom DO in October and November. The low oxygen conditions in bottom waters during summer months might have allowed the organic matter to be preserved, transported, and then respired when the water column is ventilated again, similar to the delayed decomposition reported by Officer et al. (1984) that in the Chesapeake Bay organic detritus accumulated from the previous summer and fall can last to the next year.

To further illustrate the spatial-temporal relationship between pre-DO surface Chl-*a* and bottom DO, we mapped the two variables using their monthly climatological median calculated from VIIRS and CBP data in 2011–2017. Based on our analyses above, bottom DO in August is most correlated with surface Chl-*a* of around July, so Figures 7a and 7b are used as an example of cases with phytoplankton-derived organic particles dislocated up-estuary. It is shown that at shallower regions such as the upper reach of the bay and along the coasts, the spatial patterns of Chl-*a* and DO do not match with each other, presumably owing to strong vertical mixing that dominates against oxygen consumption (Pattern 3 scenario in Figure 3). Along the deeper part of the main stem channel (see Figure 1) where influence of vertical mixing is limited, Chl-*a* appears to be inversely correlated with DO regardless of the significant difference in absolute magnitudes between the two gradients. A noteworthy feature is located at the Potomac river mouth (white dashed circle in Figure7) where spatial patterns of algal bloom in July resemble that of depressed DO in August but with

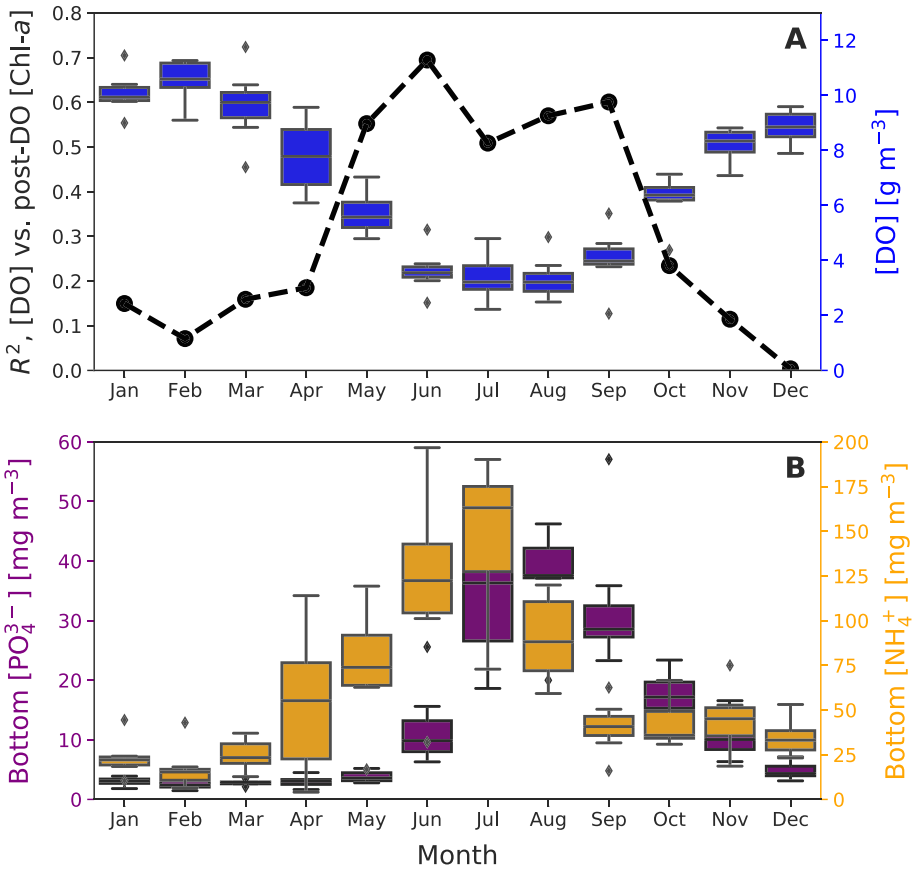

Figure 9. (a) Monthly statistics of bottom DO and correlation between DO and 8-weekly mean post-DO Chl-*a* and (b) monthly statistics of nutrient concentrations for data sampled along the main stem transect. The box shows the quartiles of each monthly data set, while the whiskers extend to show the rest of the distribution, except for points that are determined to be outliers using a method that is a function of the interquartile range.

a down-estuary shift of roughly 30–40 km depending on the choice of contour level, which agrees with the 36-km shift in August for the analysis made solely with the central transect data (Figure 6). For comparison, we also show the October DO map and the most correlated Chl-*a* map as an example of significant particulate dislocation in the down-estuary direction (Figures 7c and 7d). As discussed above, October DO is most correlated with Chl-*a* of around June–August and 46 km up-estuary. There are no sub-estuary scale spatial features that can be visually matched between the Chl-*a* and DO maps. However, taking into account the spatial shift of 46 km (about half a degree latitude), the decreasing trend of Chl-*a* from the middle to the lower bay generally agrees with the increasing trend of DO.

3.4. Feedback of Bottom Hypoxia on Surface Phytoplankton

We also analyzed the relationship between bottom DO and the surface Chl-*a* after DO sampling, hereafter referred to as post-DO Chl-*a*. Figure 8 shows their relationship using the 8-weekly mean post-DO Chl-*a* during April–September. Similar to the scatter plot between [DO] and pre-DO Chl-*a* (Figure 3), Figure 8 also exhibits three distinct patterns. Again, we focus on data within the pattern where Chl-*a* covaries with DO using the same set of criteria as we did for identifying Pattern 1 data in Figure 3. The degree of their correlation varies slightly with duration and time lag corresponding to the mean post-DO Chl-*a*, but generally the best correlation was found for the 8-weekly mean post-DO Chl-*a*.

We found that the bottom DO and the 8-weekly mean post-DO Chl-*a* are significantly and inversely correlated during May–September and much less correlated during other months (Figure 9a). The timing of higher correlation matches with the period of lowest bottom DO, as well as increased concentrations of bottom ammonium [NH_4^+] and phosphate [PO_4^{-3}] (Figure 9b). Comparison between surface and bottom

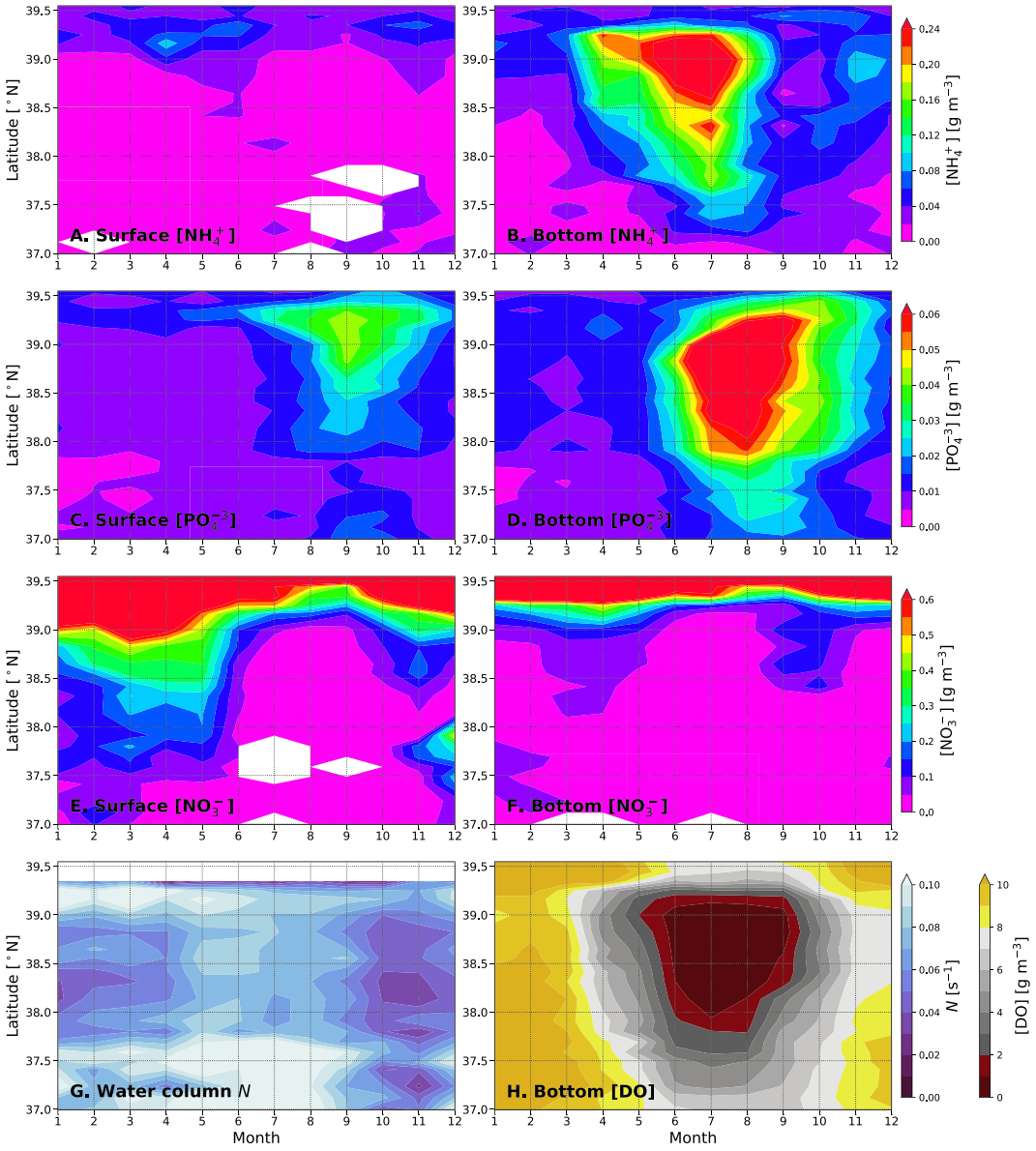

Figure 10. Comparison of Hovmoller diagrams between surface and bottom $[NH_4^+]$ (a and b), $[PO_4^{-3}]$ (c and d), and $[NO_3^-]$ (e and f). Also shown are water column stability represented by buoyancy frequency (Brunt-Visl frequency), N, across the pycnocline (g) and (h) bottom DO. Shown here are their monthly climatology calculated as median values during 2011–2017. The buoyancy frequency N is calculated based on temperature, salinity, and depth data sampled at the above- and below-pycnocline layers.

Hovmoller diagrams of monthly median $[NH_4^+]$ (Figures 10a and 10b) and $[PO_4^{-3}]$ (Figures 10c and 10d) further confirms that the nutrients are introduced to the system at the bottom, as opposed to the surface by river discharge which is the case for $[NO_3^-]$ (Figures 10e and 10f). It also shows that the rise of bottom ammonium is roughly one month ahead of that of bottom phosphate and is initiated by the establishment of stratification, as is shown by the increase of Brunt-Vaisala buoyancy frequency, N, across the pycnocline from March to May (Figure 10g). The increase in bottom ammonium thus appears to be a combined effect of organic degradation (ammonification, to be specific) and reduction in oxygen which would otherwise have oxidized the ammonium. The lack of surface $[NH_4^+]$ when bottom $[NH_4^+]$ is high (Figure 10a) might be associated with active nitrification and preferential algal uptake particularly during summer when surface phytoplankton growth is nitrogen limited (Testa et al., 2014). Bottom phosphate does not increase significantly until June when hypoxia (DO<2 g/m^3) prevails in much of the middle and upper bay (Figure 10h) and starts to drop

with reventilation of water column in September (Figures 10g and 10h). This is consistent with previous studies that low redox conditions in hypoxic waters and sediments promote release of phosphate from iron-bound phosphorus (Conley, Carstensen, et al., 2009; Conley, Björck, et al., 2009; Kemp et al., 2005; Testa & Kemp, 2012). The strong correlation between DO and post-DO Chl-*a* (Figure 9a) and the nutrient profiles (Figure 10) shown here demonstrate that recycled ammonium and hypoxia-induced phosphate at the bottom are important nutrient sources for surface phytoplankton. The 8-week time window (Figure 9) might represent an average time scale for these nutrients to return to surface and fuel further algal blooms, but the exact time scale is likely time dependent and this number must be interpreted with caution.

4. Summary

Altogether, our findings show the strong coupling between phytoplankton and bottom oxygen in the Chesapeake Bay. The strong correlation between bottom DO and satellite-derived pre-DO Chl-*a* attests that phytoplankton-derived organic matter plays a major role in fueling the consumption of bottom oxygen. Conversely, recycled ammonium and hypoxia-induced phosphate fuel the growth of phytoplankton as is demonstrated by the correlation between bottom DO and post-DO Chl-*a*. From a technical standpoint, the DO versus pre-DO Chl-*a* correlation suggests that satellite data can be useful to more accurately mapping the spatial distribution of particulate organic sinking flux. Although this correlation is manifested only when oxygen supply and consumption are balanced, that is, during warm seasons and at stations where both vertical mixing and particulate organic sinking are limited, the impact of surface algae on bottom oxygen is ubiquitous and the utility of satellite data for this purpose can be applied across all scenarios of oxygen supply and consumption. In other words, satellite-derived Chl-*a* can provide essentially a synoptic indicator of upcoming changes in bottom water oxygen demand.

Our study also suggests that spatio-temporal linkage between phytoplankton and bottom oxygen is complex and concurrently involves both physical transport and biogeochemical processes. In this regard, a limitation of this study is the lack of quantitative characterization of oxygen supply terms associated with currents and mixing and the method used in this study is not intended for predictive purposes. However, since oxygen supply and consumption are the two major terms governing the oxygen dynamics in bottom waters (Officer et al., 1984), in future research, combining high-quality satellite Chl-*a* data with physical predictive models capable of modeling changes in oxygen supply (e.g., Scully, 2013; Shen et al., 2008) is expected to yield superior hypoxia forecasts than with physical models or satellite-derived Chl-*a* data alone.

Acknowledgments
This work was supported by NOAAs Ocean Remote Sensing (ORS) Program. We thank Menghua Wang in NOAA/STAR/SOCD for providing VIIRS data. We are grateful to all scientists, crew, and staff who collected the field data and made them available through the Chesapeake Bay Program databases. All data used in this study are freely available online (data.chesapeakebay.net; field data) and (coastwatch.noaa.gov; satellite data). The contents of this article are solely the opinions of the authors and do not constitute a statement of policy, decision, or position on behalf of the NOAA or the U.S. Government.

References

Baird, D., & Ulanowicz, R. E. (1989). The seasonal dynamics of the Chesapeake Bay ecosystem. *Ecological Monographs*, *59*(4), 329–364. https://doi.org/10.2307/1943071

Bauer, J. E., Cai, W.-J., Raymond, P. A., Bianchi, T. S., Hopkinson, C. S., & Regnier, P. A. G. (2013). The changing carbon cycle of the coastal ocean. *Nature*, *504*, 61–70. https://doi.org/10.1038/nature12857

Bianchi, T., DiMarco, S., Cowan, J., Hetland, R., Chapman, P., Day, J., & Allison, M. (2010). The science of hypoxia in the northern Gulf of Mexico: A review. *Science of the Total Environment*, *408*(7), 1471–1484. https://doi.org/10.1016/j.scitotenv.2009.11.047

Boicourt, W. C., Kuzmi, M., & Hopkins, T. S. (2013). The inland sea: Circulation of Chesapeake Bay and the Northern Adriatic, *Ecosystems at the land-sea margin: Drainage basin to coastal sea* (pp. 81–129). Washington D.C.: American Geophysical Union (AGU). https://doi.org/10.1029/CE055p0081

Breitburg, D., Levin, L. A., Oschlies, A., Grégoire, M., Chavez, F. P., Conley, D. J., et al. (2018). Declining oxygen in the global ocean and coastal waters. *Science*, *359*(6371), eaam7240. https://doi.org/10.1126/science.aam7240

Cai, W.-J., Hu, X., Huang, W.-J., Murrell, M. C., Lehrter, J. C., Lohrenz, S. E., et al. (2011). Acidification of subsurface coastal waters enhanced by eutrophication. *Nature Geoscience*, *4*, 766–770. https://doi.org/10.1038/ngeo1297

Canuel, E. A., & Zimmerman, A. R. (1999). Composition of particulate organic matter in the southern Chesapeake Bay: Sources and reactivity. *Estuaries*, *22*(4), 980–994. https://doi.org/10.2307/1353077

Conley, D. J., Björck, S., Bonsdorff, E., Carstensen, J., Destouni, G., Gustafsson, B. G., et al. (2009). Hypoxia-related processes in the Baltic Sea. *Environmental Science & Technology*, *43*(10), 3412–3420. https://doi.org/10.1021/es802762a

Conley, D. J., Carstensen, J., Vaquer-Sunyer, R., & Duarte, C. M. (2009). Ecosystem thresholds with hypoxia. *Hydrobiologia*, *629*(1), 21–29. https://doi.org/10.1007/s10750-009-9764-2

Deutsch, C., Brix, H., Ito, T., Frenzel, H., & Thompson, L. (2011). Climate-forced variability of ocean hypoxia. *Science*, *333*(6040), 336–339. https://doi.org/10.1126/science.1202422

Diaz, R. J. (2001). Overview of hypoxia around the world. *Journal of Environmental Quality*, *30*(2), 275–281.

Diaz, R. J., & Rosenberg, R. (1995). Marine benthic hypoxia: A review of its ecological effects and the behavioural responses of benthic macrofauna. *Oceanography and Marine Biology*, *33*, 245–303.

Diaz, R. J., & Rosenberg, R. (2008). Spreading dead zones and consequences for marine ecosystems. *Science*, *321*(5891), 926–929. https://doi.org/10.1126/science.1156401

Dortch, Q., Rabalais, N. N., Turner, R. E., & Qureshi, N. A. (2013). Impacts of changing Si/N ratios and phytoplankton species composition, *Coastal hypoxia: Consequences for living resources and ecosystems* (pp. 37–48). Washington D.C.: American Geophysical Union (AGU). https://doi.org/10.1029/CE058p0038

Goodrich, D. M., Boicourt, W. C., Hamilton, P., & Pritchard, D. W. (1987). Wind-induced destratification in Chesapeake Bay. *Journal of Physical Oceanography*, *17*(12), 2232–2240. https://doi.org/10.1175/1520-0485(1987)017<2232:WIDICB>2.0.CO;2

Guo, X., & Valle-Levinson, A. (2008). Wind effects on the lateral structure of density-driven circulation in Chesapeake Bay. *Continental Shelf Research*, *28*(17), 2450–2471. https://doi.org/10.1016/j.csr.2008.06.008

Hagy, J. D., Boynton, W. R., & Jasinski, D. A. (2005). Modelling phytoplankton deposition to Chesapeake Bay sediments during winter spring: Interannual variability in relation to river flow. *Estuarine, Coastal and Shelf Science*, *62*(1), 25–40. https://doi.org/10.1016/j.ecss.2004.08.004

Hagy, J. D., Boynton, W. R., Keefe, C. W., & Wood, K. V. (2004). Hypoxia in Chesapeake Bay, 1950–2001: Long-term change in relation to nutrient loading and river flow. *Estuaries*, *27*(4), 634–658.

Harding Jr, L. W., Mallonee, M. E., Perry, E. S., Miller, WDavid, Adolf, J. E., Gallegos, C. L., & Paerl, H. W. (2016). Variable climatic conditions dominate recent phytoplankton dynamics in Chesapeake Bay. *Scientific Reports*, *6*, 23773.

Harvey, H. R., & Johnston, J. R. (1995). Lipid composition and flux of sinking and size-fractionated particles in Chesapeake Bay. *Organic Geochemistry*, *23*(8), 751–764. https://doi.org/10.1016/0146-6380(95)00056-K

Hoegh-Guldberg, O., & Bruno, J. F. (2010). The impact of climate change on the world's marine ecosystems. *Science*, *328*(5985), 1523–1528. https://doi.org/10.1126/science.1189930

Jiang, L., & Wang, M. (2014). Improved near-infrared ocean reflectance correction algorithm for satellite ocean color data processing. *Optics Express*, *22*(18), 21,657–21,678. https://doi.org/10.1364/OE.22.021657

Kemp, W. M., Boynton, W. R., Adolf, J. E., Boesch, D. F., Boicourt, W. C., Brush, G., et al. (2005). Eutrophication of Chesapeake Bay: Historical trends and ecological interactions. *Marine Ecology Progress Series*, *303*, 1–29.

Lee, Z. (2014). An update of the quasi-analytical algorithm (qaa_v6) [Computer software manual]. available online at www.ioccg.org/groups/software.html

Levin, L. A., & Breitburg, D. L. (2015). Linking coasts and seas to address ocean deoxygenation. *Nature Climate Change*, *5*, 401–403.

Li, Y., & Li, M. (2011). Effects of winds on stratification and circulation in a partially mixed estuary. *Journal of Geophysical Research*, *116*, C12012. https://doi.org/10.1029/2010JC006893

Li, Y., Li, M., & Kemp, W. M. (2015). A budget analysis of bottom-water dissolved oxygen in Chesapeake Bay. *Estuaries and Coasts*, *38*(6), 2132–2148.

Li, M., Zhong, L., Boicourt, W. C., Zhang, S., & Zhang, D.-L. (2007). Hurricane-induced destratification and restratification in a partially-mixed estuary. *Journal of Marine Research*, *65*, 169–192.

Marshall, H. G., Burchardt, L., & Lacouture, R. (2005). A review of phytoplankton composition within Chesapeake Bay and its tidal estuaries. *Journal of Plankton Research*, *27*(11), 1083–1102. https://doi.org/10.1093/plankt/fbi079

McManus, G. B., & Ederington-Cantrell, M. C. (1992). Phytoplankton pigments and growth rates, and microzooplankton grazing in a large temperate estuary. *Marine Ecology Progress Series*, *87*(1/2), 77–85.

ODell, J. W. (1993a). Method 360.1: Determination of ammonia nitrogen by semi-automated colorimetry.

ODell, J. W. (1993b). Method 365.1: Determination of phosphorus by semiautomated colorimetry.

Officer, C. B., Biggs, R. B., Taft, J. L., Cronin, L. E., Tyler, M. A., & Boynton, W. R. (1984). Chesapeake Bay anoxia: Origin, development, and significance. *Science*, *223*(4631), 22–27. https://doi.org/10.1126/science.223.4631.22

Scully, M. E. (2013). Physical controls on hypoxia in Chesapeake Bay: A numerical modeling study. *Journal of Geophysical Research: Oceans*, *118*, 1239–1256. https://doi.org/10.1002/jgrc.20138

Shen, J., Wang, T., Herman, J., Mason, P., & Arnold, G. L. (2008). Hypoxia in a coastal embayment of the Chesapeake Bay: A model diagnostic study of oxygen dynamics. *Estuaries Coast*, *31*(4), 652–663. https://doi.org/10.1007/s12237-008-9066-3

Sinha, E., Michalak, A. M., & Balaji, V. (2017). Eutrophication will increase during the 21st century as a result of precipitation changes. *Science*, *357*(6349), 405–408.

Testa, J. M., & Kemp, W. M. (2012). Hypoxia-induced shifts in nitrogen and phosphorus cycling in Chesapeake Bay. *Limnology and Oceanography*, *57*(3), 835–850. https://doi.org/10.4319/lo.2012.57.3.0835

Testa, J. M., Li, Y., Lee, Y. J., Li, M., Brady, D. C., Toro, D. M. D., et al. (2014). Quantifying the effects of nutrient loading on dissolved O_2 cycling and hypoxia in Chesapeake Bay using a coupled hydrodynamic biogeochemical model. *Journal of Marine Systems*, *139*, 139–158. https://doi.org/10.1016/j.jmarsys.2014.05.018

Turner, J. T. (2002). Zooplankton fecal pellets, marine snow and sinking phytoplankton blooms. *Aquatic Microbial Ecology*, *27*(1), 57–102.

Tyler, M. A., & Seliger, H. H. (1978). Annual subsurface transport of a red tide dinoflagellate to its bloom area: Water circulation patterns and organism distributions in the CBay 1. *Limnology and Oceanography*, *23*(2), 227–246. https://doi.org/10.4319/lo.1978.23.2.0227

Walker, N. D., & Rabalais, N. N. (2006). Relationships among satellite chlorophylla, river inputs, and hypoxia on the Louisiana continental shelf, Gulf of Mexico. *Estuaries Coast*, *29*(6), 1081–1093. https://doi.org/10.1007/BF02781811

Wei, J., Lee, Z., & Shang, S. (2016). A system to measure the data quality of spectral remote-sensing reflectance of aquatic environments. *Journal of Geophysical Research: Oceans*, *121*, 8189–8207. https://doi.org/10.1002/2016JC012126

White, J. R., & Roman, M. R. (1992). Seasonal study of grazing by metazoan zooplankton in the mesohaline Chesapeake Bay. *Marine Ecology Progress Series*, *86*(3), 251–261.

Zheng, G., & DiGiacomo, P. M. (2017a). Remote sensing of chlorophyll-a in coastal waters based on the light absorption coefficient of phytoplankton. *Remote Sensing of Environment*, *201*, 331–341. https://doi.org/10.1016/j.rse.2017.09.008

Zheng, G., & DiGiacomo, P. M. (2017b). Uncertainties and applications of satellite-derived coastal water quality products. *Progress in Oceanography*, *159*, 45–72. https://doi.org/10.1016/j.pocean.2017.08.007

Zheng, G., Stramski, D., & DiGiacomo, P. M. (2015). A model for partitioning the light absorption coefficient of natural waters into phytoplankton, nonalgal particulate, and colored dissolved organic components: A case study for the Chesapeake Bay. *Journal of Geophysical Research: Oceans*, *120*, 2601–2621. https://doi.org/10.1002/2014JC010604

Zimmerman, A. R, & Canuel, E. A (2001). Bulk organic matter and lipid biomarker composition of Chesapeake Bay surficial sediments as indicators of environmental processes. *Estuarine, Coastal and Shelf Science*, *53*(3), 319–341. https://doi.org/10.1006/ecss.2001.0815